



Full Length Article

Study on top sulfur hyperdoping layer covering microstructured Si by fs-laser irradiation

Ke Wang^{a,b}, Jinsong Gao^{a,b}, Haigui Yang^{a,*}, Xiaoyi Wang^{a,*}, Yanchao Wang^{a,b}, Zhuo Zhang^a

^a Key Laboratory of Optical System Advanced Manufacturing Technology, Changchun Institute of Optics, Fine Mechanics and Physics, Chinese Academy of Sciences, Changchun 130033, China

^b University of the Chinese Academy of Sciences, Beijing 100039, China

ARTICLE INFO

Keywords:

Sulfur hyperdoping
Silicon
Femtosecond laser
Infrared absorption

ABSTRACT

We studied the infrared absorption of a top sulfur hyperdoping layer covering an fs-laser irradiated microstructured Si substrate. To clarify the hyperdoping concentration distributions, and to find out how the top hyperdoping layer affects infrared absorption from 1200 to 2000 nm, a continuous etching treatment was utilized. Then we interpreted the thermal stabilization of both infrared absorption and sulfur hyperdoping concentration. The fundamental cause for infrared-absorption degradation under thermal annealing was explained. Furthermore, we discussed in detail how the interaction between the top hyperdoping layer and surface microstructure contributed to the high infrared absorption by a series of theoretical simulations using a finite-difference time-domain method. A strong localization of an incident electromagnetic wave was observed around the top sulfur hyperdoping layer covering microstructured Si, which played a critical role in improving infrared absorption. The results in this paper are especially beneficial to the subsequent fabrication of photoelectric devices and infrared response improvement.

1. Introduction

Developing low-cost infrared imaging systems or sensors is of great interest for wide applications in the telecommunications, security, and automotive industries. Silicon (Si), as the second-most-abundant element in the Earth's crust, satisfies the low-cost and on-chip complementary metal-oxide semiconductor (CMOS) compatibility criteria. However, its wide intrinsic band gap of 1.12 eV limits the infrared photoresponse of Si devices to roughly less than 1100 nm. Several attempts to extend its photoresponse limit to a longer infrared wavelength involve forming heterostructures with traditional narrow-band-gap Ge or SiGe materials [1,2], plasmonic metallic nanoantennas [3–5], and incorporating chalcogen hyperdoping in Si [6–13]. By improving infrared light absorption ability, all these approaches can result in extending the infrared response of Si-based devices, although they are based on different physical mechanisms.

A promising approach to extend the infrared photoresponse is incorporating chalcogen hyperdoping in a Si substrate [9,10]. The Chalcogen hyperdoping is able to create a dopant concentration as high as 10^{20} cm^{-3} , far beyond their solid solubility limit. In the case of the hyperdoping, electron-electron interaction couples the energy levels into a band, often referred to as an impurity or intermediate band

[11,12], which extends the long-wavelength limit of infrared absorption through sub-band-gap absorption. In addition to the fabrication of the so-called laser-induced periodic surface structures which is used for optical storage and planar optoelectronic circuits, such as self-organized periodic structures [14], nanohillocks and nanoholes [15], femtosecond-laser (fs-laser) irradiation can incorporate chalcogen hyperdoping effectively. Different from ion implantation [7,8], hyperdoping via fs-laser irradiation is accompanied by surface microstructure generation due to high-intensity laser ablation. This leads to a much higher absorption (roughly above 90%) compared with that prepared by ion implantation [7,8]. The physical mechanisms of the hyperdoping-induced infrared absorption have been studied by many researchers through experiments and theoretical calculations [6–8,11–13]. However, in order to extract satisfactory infrared photoresponse in microstructured Si, clarifying the interaction between top hyperdoping layer and surface microstructure contributing infrared absorption, and achieving a further high infrared absorption while maintaining a small surface roughness is greatly desired.

In this study, we investigated the infrared-absorption enhancement occurring in a top sulfur hyperdoping layer covering microstructured Si by fs-laser irradiation. Firstly, we clarified hyperdoping concentration distributions, and how the top hyperdoping layer affects infrared

* Corresponding authors.

E-mail addresses: yanghg@ciomp.ac.cn (H. Yang), wangxiaoyi1977@sina.com (X. Wang).

<https://doi.org/10.1016/j.apsusc.2018.09.125>

Received 22 May 2018; Received in revised form 18 July 2018; Accepted 14 September 2018

Available online 15 September 2018

0169-4332/ © 2018 Elsevier B.V. All rights reserved.

absorption from 1200 to 2000 nm by a continuous etching treatment. We then studied the thermal stabilization of both infrared absorption and sulfur hyperdoping concentration. Finally, we discussed in detail how the interaction between the top hyperdoping layer and surface microstructure contributes to the high infrared absorption through a series of theoretical simulations using a finite-difference time-domain method.

2. Experiment design and fabrication

In this experiment, a single-sided polished and boron-doped Si substrate wafer with a resistivity of $10 \Omega \text{ cm}$ was used to cut to a size of $2 \times 2 \text{ cm}^2$. After cleaning of organic and metallic surface contamination, the wafer was immediately placed on a translation stage in a vacuum chamber evacuated to less than $1 \times 10^{-3} \text{ Pa}$. The chamber was filled with high-purity SF_6 gas at a pressure of $5 \times 10^4 \text{ Pa}$. The wafer was irradiated by a 1-kHz, 100-fs, 800-nm Ti:sapphire laser with a snake-scanned route under high and low laser fluence, separately. The laser was then focused vertically on a $150\text{-}\mu\text{m}$ -diam spot on the surface of the sample by a lens with a focal length of 0.5 m. After fs-laser processing, the top hyperdoping layer of microstructured Si sample was etched by reactive ion etching (RIE) to study its optical properties. Moreover, a thermal annealing treatment was performed at 1075 K in a furnace with N_2 ambient for 30 min to study its thermal stabilization.

To analyze the absorption of microstructured Si, we measured the integrated reflectance (R) and transmittance (T) spectra between 500 and 2000 nm in a Lambda-1050 spectrometer (PerkinElmer, USA) equipped with a 160-mm integrating sphere. Then the integrated absorptance (A) spectra were extracted through $A = 1 - R - T$. Furthermore, we characterized surface morphology of the sample using scanning electron microscopy (SEM), also sulfur hyperdoping concentration distribution using secondary-ion mass spectrometry (SIMS) and crystal properties in the surface layer using confocal Raman spectroscopy with a 632 nm laser excitation.

3. Results and discussion

A schematic drawing of the fs-laser irradiation method is shown in Fig. 1(a). And the surface microstructures illustrated in diagram of Fig. 1(b) can be formed. Fig. 1(c) shows the fabricated microstructured surface measuring $2 \times 2 \text{ cm}^2$ on the Si substrate. The integrated reflectance of the microstructured surface in the visible region is less than 5% due to the anti-reflection microstructures, and therefore the surface looks very black. Fig. 2(a) and (b) show the surface microstructure

morphology from different views. After fs-laser irradiation, two typical features on the microstructured surface were observed: one is that an array of micrometer-sized conical spikes with quasi-periodic distribution was created, and the other is that there was a large amount of nanoscale particles spread across a surface of conical spikes. Since conical spikes induced by fs-laser irradiation were first observed by Mazur's group [13], the formation mechanisms and the influence of experimental conditions on surface morphology have been widely studied by many researchers [16–21]. In addition to laser parameters such as fluence and pulse duration, the ambient gas plays a critical role in the spike microstructure morphology. The surface irradiated in N_2 or vacuum ambient has even blunter microstructures [20,21]. However, the conical spikes formed in SF_6 ambient in this study exhibit much sharpness, as shown in Fig. 2(a) and (b). In SF_6 ambient, high-intensity laser pulses can ablate Si surface and simultaneously dissociate SF_6 , resulting in a chemical reaction between Si and SF_6 , by which the radicals etch Si via volatile SiF_4 formation. Besides that, laser pulse can also enhance the reactivity by inducing vibrationally excited SF_6 [22].

When fs-laser pulses interact with Si in SF_6 ambient, on the other hand, the ultra-fast melting and ultra-fast condensation will bind sulfur atoms generated by dissociated SF_6 to form a nonequilibrium hyperdoping layer on the Si surface. Fig. 2c presents the concentration profile of doped sulfur atoms distributed in the surface layer after fs-laser irradiation. It is determined by a SIMS method using a CAMECA 6F with a 25° incident angle and 14.5 keV Cs⁺ beam. The detected area is a $30 \mu\text{m}$ -diameter circle containing several tens of spikes. Therefore, these results reflect the average concentration of sulfur in conical spikes. In Fig. 2c the sulfur doped depth (thickness of top hyperdoping layer cover on the microstructure) is defined as the depth (thickness) along the vertical direction of the lateral surface of the conical structures. The doped depth is then determined by “Depth = $L \times \sin \theta$ ”, where L is the measured longitudinal depth, and θ is half of the cone angle of the microstructure in the detected area. According to the Fig. 2(b) and (e), we set θ to 15° for both before and after etching respectively, which is half of the average angle of the microstructures in the detected area. Similar hyperdoping concentration distribution determined by SIMS method has been demonstrated by Zhuang et al [20]. From Fig. 2(c), we can see that sulfur atoms have been hyperdoped into the surface layer of the conical spikes shown in Fig. 2(a) and (b). Sulfur dopant concentration in the uppermost 200-nm depth is more than 10^{20} cm^{-3} , several orders of magnitude greater than its solid solubility limit of $3 \times 10^{16} \text{ cm}^{-3}$ in Si crystals [23–26]. Thus, fs-laser irradiation can simultaneously realize surface microstructuring and atom hyperdoping.

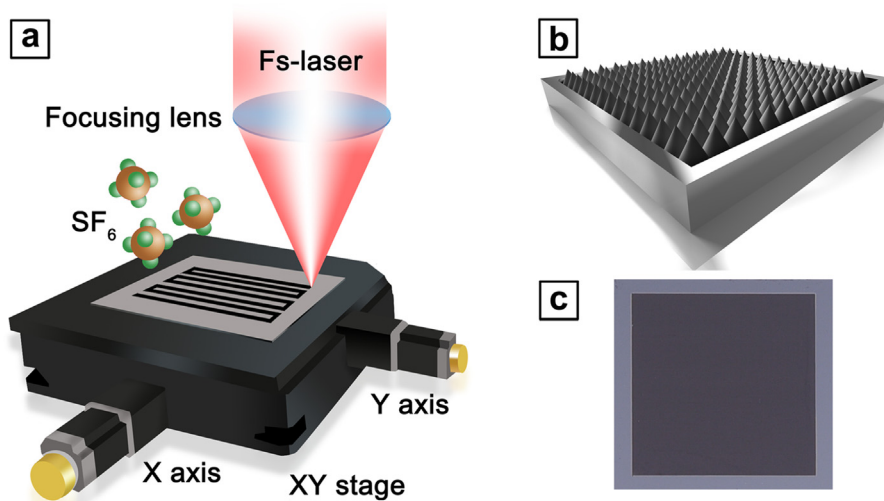


Fig. 1. (a) Schematic of fs-laser irradiation for microstructured Si fabrication. (b) Diagram of surface microstructures. (c) Photograph of fabricated microstructured Si surface.

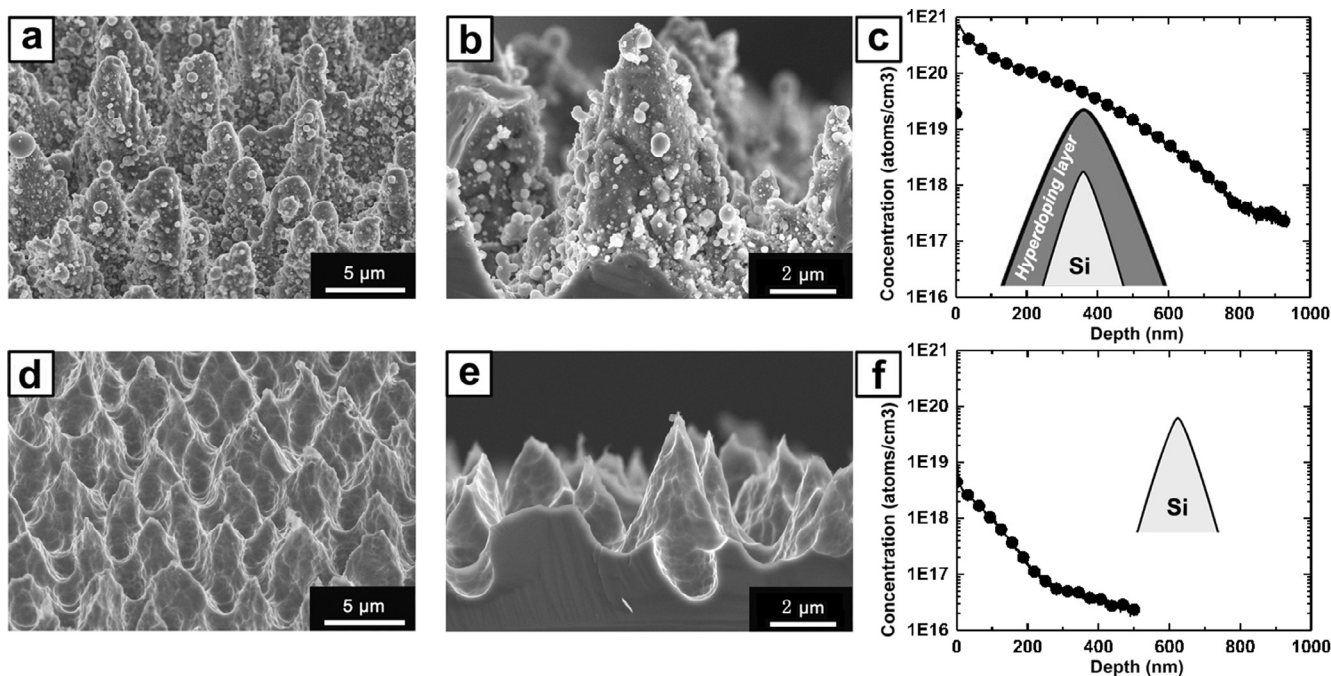


Fig. 2. (a,b) Scanning-electron-microscopy (SEM) images of microstructured Si surface from different views: (a) tilt view (45°) and (b) side view. (c) Concentration profile of top sulfur hyperdoping layer after fs-laser irradiation. (d,e) SEM images of microstructured Si surface after 4 min of etching: (d) tilt view (45°) and (e) side view. (f) Concentration profile of top sulfur hyperdoping layer after 4 min of etching.

As a highlight of this study, we emphasized on investigating how the top hyperdoping layer affects infrared absorption. In order to clarify this, we gradually cut down the top sulfur hyperdoping layer by RIE with a 50-W plasma in SF₆ ambient. To better understand the change of the top sulfur hyperdoping layer, after 4 min of etching we took the surface morphology and sulfur concentration profile of microstructured Si, as shown in Fig. 2(d–f). When compared with the sample without etching treatment shown in Fig. 2(a) and (b), it is clear that the etching treatment removed large amounts of nanoscale particles covering the spike surface, sharpened the spike structures, and, most importantly, reduced the spike height. Fig. 2(f) shows that the sulfur concentration in the top hyperdoping layer drastically decreases to less than $1 \times 10^{19} \text{ cm}^{-3}$. This means that the top sulfur hyperdoping layer depth of approximately 600-nm is removed after 4 min of etching, as seen by comparing Fig. 2(c) and (f).

Fig. 3 shows the reflection, transmission, and absorption spectra of microstructured Si as a function of etching time. Both of the average absorbance in the short-wavelength region from 500 to 1000 nm corresponding to the intrinsic absorption of Si, and in the infrared region from 1200 to 2000 nm, are summarized in Fig. 3(d). For the irradiated microstructured Si without etching treatment, its infrared absorbance from 1200 to 2000 nm is close to 90%, which is much higher than that of the non-irradiated Si at 5%. Generally, the spike microstructures seen in Fig. 2(a) and (b) can reduce surface reflection by building a grade index from the air to Si surface and enhance the natural linear absorption of Si by multiple reflections between microstructured surfaces. In addition to microstructure function, another main contribution to a large enhancement of infrared absorption is attributed to the top sulfur hyperdoping layer formed by fs-laser irradiation. The physical origin of

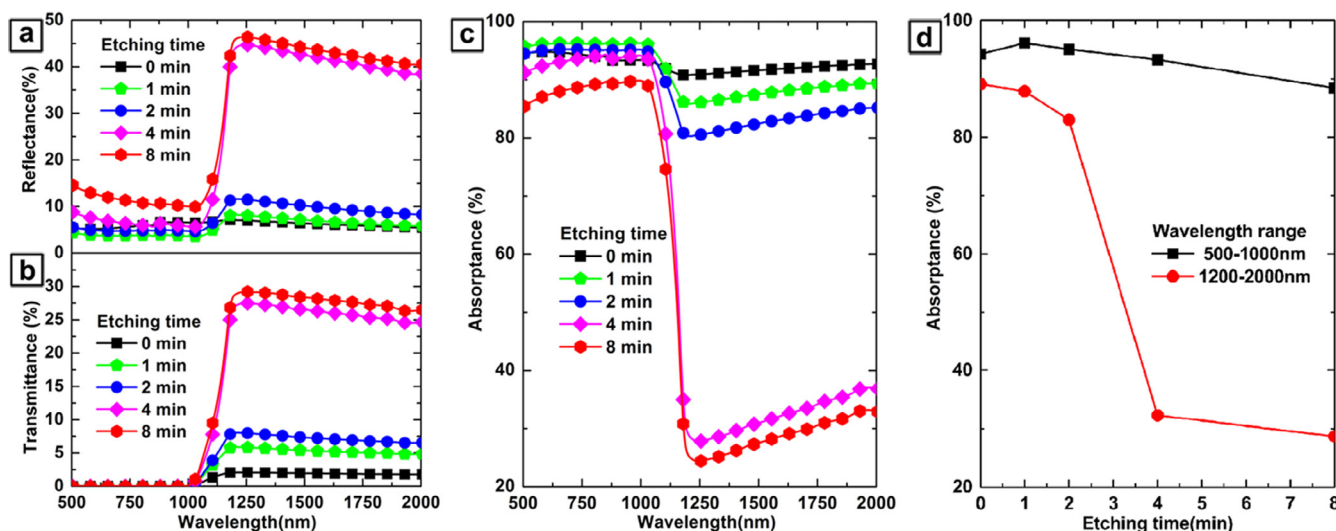


Fig. 3. (a) Reflection, (b) transmission, and (c) absorption spectra of microstructured Si as a function of etching time. (d) Average absorbance in the wavelength ranges 500–1000 and 1200–2000 nm as a function of etching time.

infrared absorption from sulfur hyperdoping has been studied theoretically [11,12]. At a low concentration of $3 \times 10^{16} \text{ cm}^{-3}$, several discrete impurity energy levels in the Si band gap have been identified [27,28]. In contrast, in the case of hyperdoping, electron-electron interaction couples the energy levels into a band, often referred to as an impurity or intermediate band [11,12]. This intermediate band is close to the conduction-band minimum of Si, and its bandwidth and location have a linear dependence on doping concentration. The formation of an intermediate band results in sub-band-gap absorption and extends the long-wavelength limit of infrared absorption to 2000 nm.

From the absorption dependence on etching times, we found that the intrinsic absorption of Si in the short-wavelength region from 500 to 1000 nm is not sensitive to etching times. Even though 8 min of etching was done, its average absorbance is still close to 90%. However, it exhibits a completely different dependence behavior in the infrared region from 1200 to 2000 nm beyond the Si absorption limit. At the initial stage of 2 min of etching, the infrared absorption still maintained a high value of approximately 85%. As the etching proceeds, the top sulfur hyperdoping layer will be cut down. The absorbance drastically decreases to less than 35% after 4 min of etching and tends to be stable after 8 min of etching. The different changes in two-wave-band absorption with etching time indicate that the reduction in infrared absorption from 1200 to 2000 nm is derived from the thickness reduction of the top sulfur hyperdoping layer, instead of the change of surface microstructure shown in Fig. 2.

Additionally, we investigated the thermal stabilization of both infrared absorption and sulfur hyperdoping concentration, as illustrated

in Fig. 4(a) and (b). After 1075-K thermal annealing for 30 min, the average infrared absorbance from 1200 to 2000 nm significantly decreases by 60%. However, the sulfur atom is only diffused slightly toward the deeper position and it still exhibits a hyperdoping with a concentration beyond 10^{20} cm^{-3} in the uppermost several hundred nanometers of depth. To further clarify thermal annealing effects on microstructured Si, we investigated its crystalline morphology before and after thermal treatment by Raman measurements. As shown in Fig. 4(c), before thermal treatment it exhibits several Raman modes corresponding to conventional crystalline Si (Si-I), pressure-induced crystalline phases (Si-III and Si-XII) and amorphous Si (a-Si) by fs-laser-induced sub-surface phase transformations [29]. Among them, a-Si causes a large number of structure defects and a high density of recombination sites [29], Si-XII has an indirect band gap of 230 meV [30], and Si-III is a p-type semimetal [31]. After thermal treatment, however we can clearly see from Fig. 4(c) that, a-Si, Si-III, and Si-XII are converted to Si-I, resulting in a great increase in Raman modes at 303 cm^{-1} and 522 cm^{-1} .

One speculation that exists now is that the large drop in infrared absorption after thermal treatment comes from the suppression of a-Si, Si-III and Si-XII phases. Franta et al have indicated that a-Si, Si-III and Si-XII phases can also be suppressed by a nanosecond-laser annealing, but the suppression has no obvious influence on infrared absorption of microstructure Si [32]. Therefore, we speculate that annealing-induced infrared absorption reduction derives from the change of the existence configurations of hyperdoping sulfur in Si material. After high-intensity fs-laser irradiation, sulfur hyperdoping in a Si lattice is in a highly non-

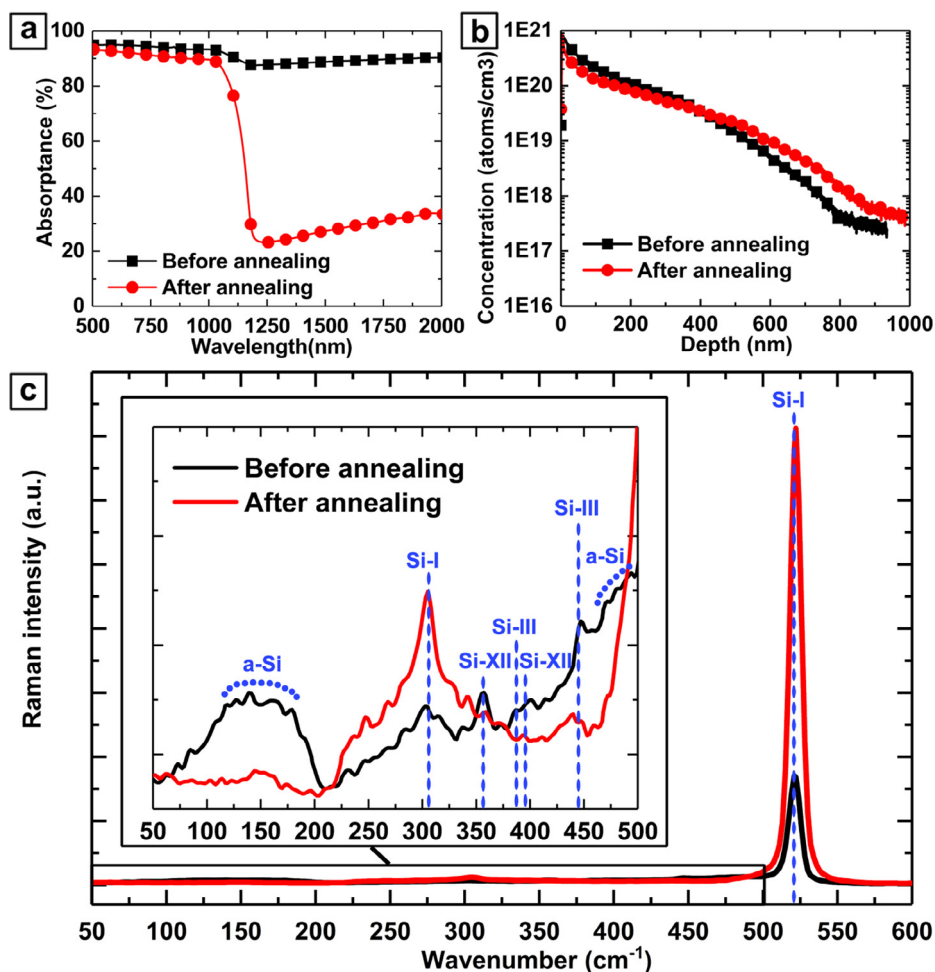


Fig. 4. (a) Absorption spectra, (b) sulfur hyperdoping concentration profile, and (c) Raman spectra of hyperdoped microstructured Si before and after annealing. Inset: Raman modes corresponding to conventional crystalline Si (Si-I), pressure-induced crystalline phases (Si-III and Si-XII), and amorphous Si (a-Si).

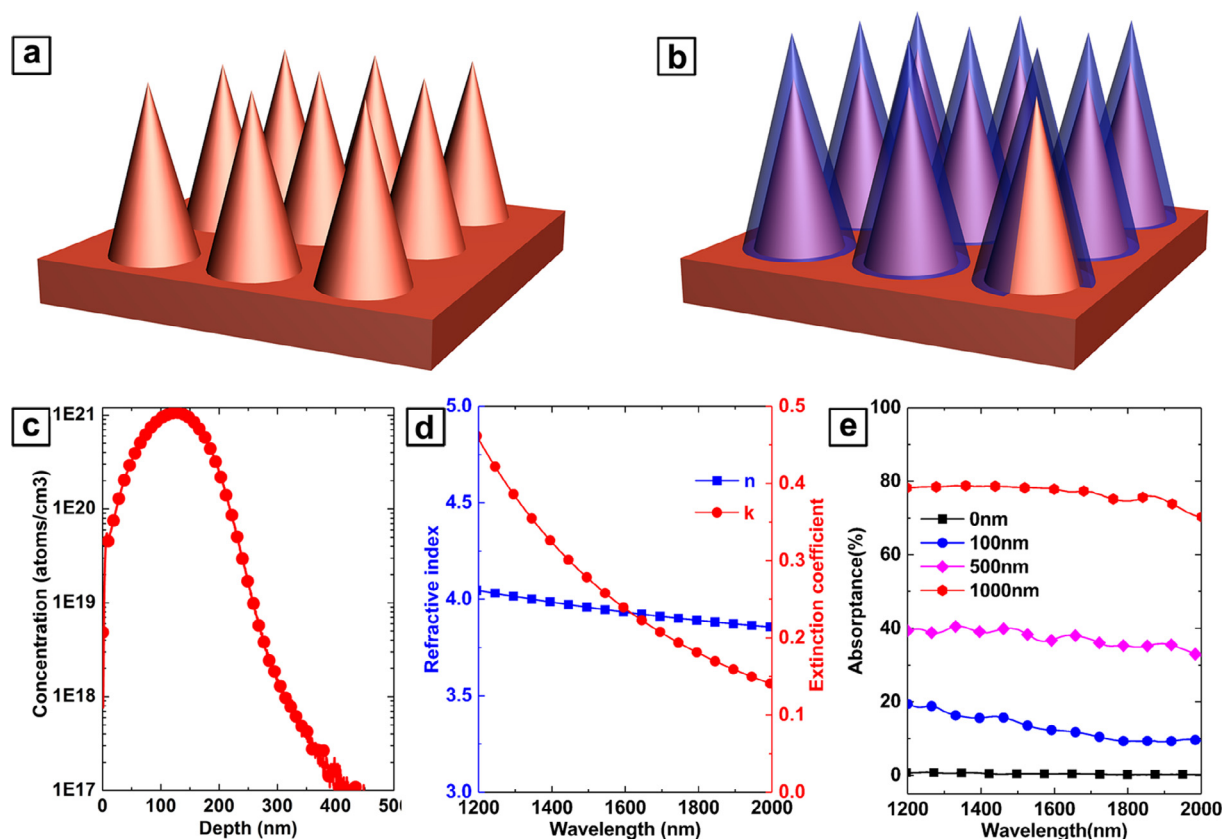


Fig. 5. (a,b) Theoretical models of microstructure Si used in the simulation: periodically arranged Si-based conical spike (a) without and (b) with top sulfur hyperdoping layer. (c) Concentration profile of a flat sulfur doping layer on Si substrate fabricated by sulfur-ion implantation. (d) Extracted optical constants of sulfur doping layer used in the simulation. (e) Simulated infrared absorption spectra of spike microstructures without and with different thicknesses (0, 100, 500, and 1000 nm) of sulfur hyperdoping layer.

equilibrium state. During thermal annealing, sulfur atoms prefer moving to a thermodynamically stable state. From first-principle calculations [12], it has been predicted that the atomic structure of hyperdoped sulfur in a Si lattice is changed via two types of structural transformations during thermal annealing process. One is that the higher-energy interstitial configurations transform to the lowest-energy interstitial ones, and the other is that the quasi-substitutional configurations transform to the lowest-energy interstitial ones. Therefore, combined with Fig. 4(b) and (c), we think that the transformation from higher-energy interstitial and quasi-substitutional configurations to the lowest-energy interstitial ones is responsible for annealing-induced infrared absorption reduction. In other words, strong infrared absorption is dependent on not only sulfur hyperdoping concentration, but its existence configurations in the Si material.

In order to further clarify the contribution of the top sulfur hyperdoping layer on infrared absorption, we performed a three-dimensional finite-difference time-domain (FDTD) simulation to study the optical characteristics of microstructured Si. As shown in Fig. 5(a), the theoretical modes are composed of periodically arranged Si-based conical spikes without a top sulfur hyperdoping layer, where the height (H) and half of the top angle (θ) are set as $4\ \mu\text{m}$ and 15° , respectively, roughly close to the real spike size shown in Fig. 2. Hyperdoping layers with thicknesses (HLT) of 100, 500, and 1000 nm are covering the spikes in Fig. 5(b), resulting in the height of spikes increasing by approximately 4.5, 6, and $8\ \mu\text{m}$, respectively, according to $H = \text{HLT} / \sin \theta$. Compared with the real microstructures shown in Fig. 2, in the theoretical mode, we omitted the randomly-distributed irregular nanoparticles adhering the microspikes to simplify the calculations,

which possibly leads to a calculated absorption lower than the actual. In the theoretical simulation, the periodic boundary conditions were used for a unit cell in the x - y plane, and perfectly matched layers (PMLs) are applied along the z axis. Incident light with a wavelength range of 1200–2000 nm propagates along the negative z -axis direction, with the electrical field polarization in the x direction.

The optical constant of the top sulfur hyperdoping layer formed by fs-laser irradiation is a key parameter in the simulation. However, it has never been reported to our knowledge, perhaps because of the microstructured surface impact. We tried to extract it using ellipsometry measurements, but, unfortunately, the anti-reflection property of the microstructured surface caused an overly weak reflection signals to be well detected. We used another method of sulfur ion implantation to fabricate a flat sulfur doping layer on the Si substrate. The concentration profile in Fig. 5(c) implies that an ion implantation method can also lead to a hyperdoping layer with a concentration higher than $10^{20}\ \text{cm}^{-3}$, which is similar to that achieved by fs-laser irradiation, except for the difference in doping depth. Thus, it is reasonable that the extracted optical constants in Fig. 5(d) of the sulfur hyperdoping layer from ion implantation are used in the simulation.

Fig. 5(e) shows the simulated infrared absorption spectra of spike microstructures with and without different thicknesses of the sulfur hyperdoping layer, from which we can see clearly that the sulfur hyperdoping layer plays a critical role in infrared-absorption enhancement. When the spike microstructure is not covered with a hyperdoping layer, its infrared absorption from 1200 to 2000 nm is very weak even though it has an anti-reflection function. However, the infrared absorption significantly increases when only a 100-nm-thick sulfur

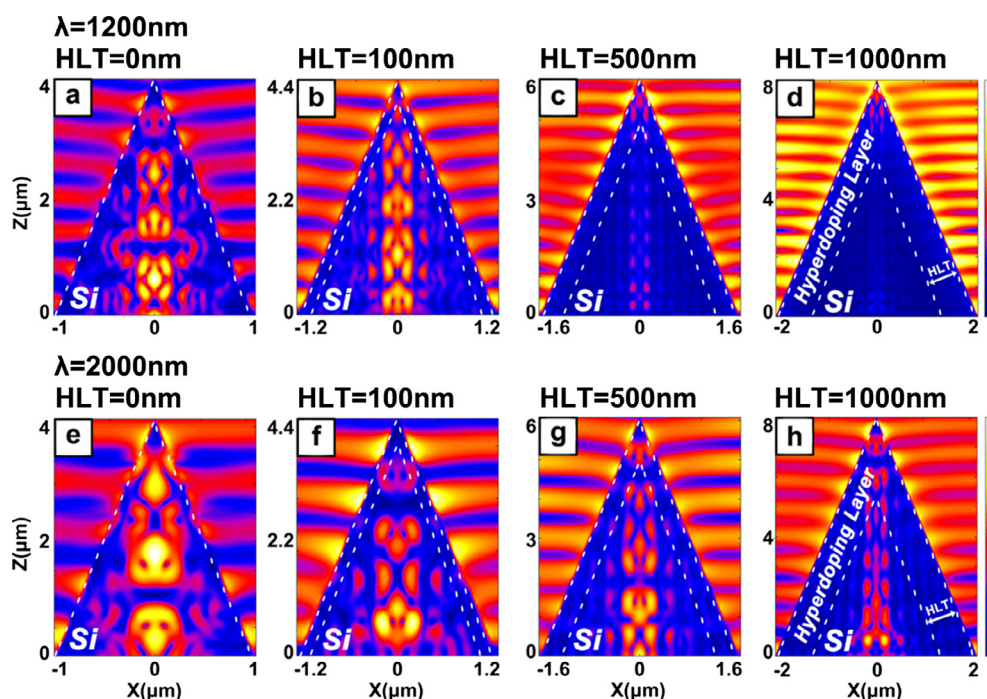


Fig. 6. (a–h) Cross-sectional (in the x - z plane) electric field distributions of the microstructures at incident wavelengths of 1200 and 2000 nm. Hyperdoping layer thicknesses (HLT) are 0, 100, 500, and 1000 nm. Color bar denotes the relative electric field intensity. (For interpretation of the references to colour in this figure legend, the reader is referred to the web version of this article.)

hyperdoping layer is covering the spikes. The thicker the sulfur hyperdoping layer becomes, the more absorption enhancement can be achieved, which is quantitatively consistent with observations in the hyperdoping layer etching experiments. In addition, as shown in Fig. 6, the electric-field distributions without a hyperdoping layer are completely distinguished from those with a hyperdoping layer. We will explain next how infrared absorption is significantly enhanced after a hyperdoping layer is covering the spikes.

It is known that the spike structure provides an increasing cross-section width from its top to bottom, resulting in a height-dependent grade index. This grade index, independent of wavelength, leads to an electric field localization in a broadband wavelength range from 1200 to 2000 nm. By comparing electric field distributions, it is found that the great difference is the localization position. In the case of a pure Si spike structure not covered by a hyperdoping layer, the electric field is strongly localized inside the spikes, because pure Si is highly transparent for wavelengths longer than 1200 nm, and strong localization still cannot enhance its absorption. In contrast, with increasing hyperdoping layer thickness, the electric fields are mainly localized around the hyperdoping layer surface instead of the cores of the spikes covered with a sulfur hyperdoping layer. Owing to the optical properties of the hyperdoping layer, the localized electromagnetic wave energy can be efficiently consumed inside the hyperdoping layer and cannot be coupled into the spike core. As a result, with increasing sulfur hyperdoping layer thickness, the absorption of microstructured Si in the near-infrared region became stronger. The simulated electric field distributions provided powerful evidence that the sulfur hyperdoping layer makes a dominant contribution to the broadband and high absorption in the infrared region by a combination of spike microstructures.

4. Conclusion

In conclusion, we have successfully demonstrated that infrared absorption from 1200 to 2000 nm in microstructured Si was strongly dependent on the top sulfur hyperdoping layer created by fs-laser irradiation. We found that etching treatment removed the top sulfur hyperdoping layer, resulting in a serious reduction of infrared absorption, from which it was proved that infrared absorption had originated

from a sulfur-hyperdoping-introduced intermediate band in the Si band gap. In addition, from SIMS measurements and Raman spectra we surmised that thermal-annealing-induced infrared absorption reduction was most likely derived from the change of the existence configurations of hyperdoping sulfur in the Si lattice. Therefore, we concluded that strong infrared absorption was dependent on not only the sulfur hyperdoping concentration, but also its existence state in the Si material. We further clarified the contribution of conical spike microstructures to high infrared absorption by a combination of theoretical simulations. From numerical simulation results, we concluded that an incident electromagnetic wave was strongly localized around the top sulfur hyperdoping layer covering microstructured Si, significantly improving the infrared absorption.

Acknowledgements

This work was supported by the National Natural Science Foundation of China (Grant Nos. 61675199 and U1435210).

Competing financial interests

The authors declare no competing financial interests.

References

- [1] Y. Kang, H.D. Liu, M. Morse, M.J. Paniccia, M. Zadka, Monolithic germanium/silicon avalanche photodiodes with 340 GHz gain-bandwidth product, *Nat. Photonics* 3 (2008) 59.
- [2] J. Michel, J. Liu, L.C. Kimerling, High-performance Ge-on-Si photodetectors, *Nat. Photonics* 4 (2010) 527.
- [3] M.W. Knight, H. Sobhani, P. Nordlander, N.J. Halas, Photodetection with active optical antennas, *Science* 332 (2011) 702.
- [4] A. Sobhani, M.W. Knight, Y.M. Wang, B. Zheng, N.S. King, L.V. Brown, Z. Fang, P. Nordlander, N.J. Halas, Narrowband photodetection in the near-infrared with a plasmon-induced hot electron device, *Nat. Commun* 4 (2013) 1643.
- [5] Y. Qu, Q. Li, H. Gong, K. Du, S. Bai, D. Zhao, H. Ye, M. Qiu, Spatially and spectrally resolved narrowband optical absorber based on 2D grating nanostructures on metallic films, *Adv. Opt. Mater.* 4 (2016) 480.
- [6] M.A. Sheehy, B.R. Tull, C.M. Friend, E. Mazur, Chalcogen doping of silicon via intense femtosecond-laser irradiation, *Mater. Sci. Eng., B* 137 (2007) 289.
- [7] T.G. Kim, J.M. Warrender, M.J. Aziz, Strong sub-band-gap infrared absorption in silicon supersaturated with sulfur, *Appl. Phys. Lett.* 88 (2006) 1850.
- [8] B.P. Bob, A. Kohno, S. Charnvanichborikarn, J.M. Warrender, I. Umezu, M. Tabbal,

- J.S. Williams, M.J. Aziz, Fabrication and subband gap optical properties of silicon supersaturated with chalcogens by ion implantation and pulsed laser melting, *J. Appl. Phys.* 107 (2010) 123506.
- [9] A.J. Said, D. Recht, J.T. Sullivan, J.M. Warrender, T. Buonassisi, P.D. Persans, M.J. Aziz, Extended infrared photoresponse and gain in chalcogen-supersaturated silicon photodiodes, *Appl. Phys. Lett.* 99 (2011) 1850.
- [10] L. Du, Z. Wu, R. Li, F. Tang, Y. Jiang, Near-infrared photoresponse of femtosecond-laser processed Se-doped silicon n⁺-n photodiodes, *Opt. Lett.* 41 (2016) 5031.
- [11] H. Shao, C. Liang, Z. Zhu, B.Y. Ning, X. Dong, X.J. Ning, Z. Li, Z. Jun, Hybrid functional studies on impurity-concentration-controlled band engineering of chalcogen-hyperdoped silicon, *Appl. Phys. Exp.* 6 (2013) 5801.
- [12] H. Shao, Y. Li, J. Zhang, B.Y. Ning, W. Zhang, X.J. Ning, Z. Li, Z. Jun, Physical mechanisms for the unique optical properties of chalcogen-hyperdoped silicon, *EPL* 99 (2012) 670.
- [13] T.-H. Her, R.J. Finlay, C. Wu, S. Deliwala, E. Mazur, Microstructuring of silicon with femtosecond laser pulses, *Appl. Phys. Lett.* 73 (1998) 1673.
- [14] S.H. Messaddeq, R. Vallée, P. Soucy, M. Bernier, M. El-Amraoui, Y. Messaddeq, Self-organized periodic structures on Ge-S based chalcogenide glass induced by femtosecond laser irradiation, *Opt. Exp.* 20 (2012) 29882.
- [15] A. Velea, M. Popescu, F. Sava, A. Lőrinczi, I.D. Simandan, G. Socol, I.N. Mihailescu, N. Stefan, F. Jipa, M. Zamfirescu, A. Kiss, V. Braic, Photoexpansion and nano-lenslet formation in amorphous As₂S₃ thin films by 800 nm femtosecond laser irradiation, *J. Appl. Phys.* 112 (2012) 033105.
- [16] R. Younkin, E. Mazur, J.E. Carey, C. Crouch, J.A. Levinson, C.M. Friend, Infrared absorption by conical silicon microstructures made in a variety of background gases using femtosecond-laser pulses, *J. Appl. Phys.* 93 (2003) 2626.
- [17] M.A. Sheehy, L. Winston, J.E. Carey, C.M. Friend, E. Mazur, Role of the background gas in the morphology and optical properties of laser-microstructured silicon, *Chem. Mater.* 17 (2005) 3582.
- [18] Y. Peng, Y.Y. Zhou, X.Q. Chen, Y.M. Zhu, The fabrication and characteristic investigation of microstructured silicon with different spike heights, *Opt. Commun.* 334 (2015) 122.
- [19] J. Yang, F. Luo, T.S. Kao, X. Li, G.W. Ho, J. Teng, X. Luo, M. Hong, Design and fabrication of broadband ultralow reflectivity black Si surfaces by laser micro/nanoprocessing, *Light. Sci. Appl.* 3 (2014) e185.
- [20] X. Dong, N. Li, Z. Zhu, H. Shao, X. Rong, C. Liang, H. Sun, G. Feng, L. Zhao, J. Zhuang, A nitrogen-hyperdoped silicon material formed by femtosecond laser irradiation, *Appl. Phys. Lett.* 104 (2014) 091907.
- [21] C.H. Li, J.H. Zhao, Q.D. Chen, J. Feng, W.T. Zheng, H.B. Sun, Infrared absorption of femtosecond laser textured silicon under vacuum, *IEEE Photonic. Tech. Lett.* 27 (2015) 1481.
- [22] T.J. Chuang, Multiple photon excited SF₆ interaction with silicon surfaces, *J. Chem. Phys.* 74 (1981) 1453.
- [23] R.O. Carlson, R.N. Hall, E.M. Pell, Sulfur in silicon, *J. Phys. Chem. Solids* 8 (1959) 81.
- [24] F.A. Trumbore, Solid solubilities of impurity elements in germanium and silicon, *Bell System Tech. J.* 39 (1960) 205.
- [25] P.W. Mason, H.J. Sun, T.C. Han, B. Ittermann, S.S. Ostapenko, G.D. Watkins, L. Jeyanathan, M. Singh, G. Davies, E.C. Lightowers, Sulfur-related metastable luminescence center in silicon, *Phys. Rev. B* 58 (1998) 7007.
- [26] Y.T. Lin, N. Mangan, S. Marbach, T.M. Schneider, G. Deng, S. Zhou, M.P. Brenner, E. Mazur, Creating femtosecond-laser-hyperdoped silicon with a homogeneous doping profile, *Appl. Phys. Lett.* 106 (2015) 3582.
- [27] G.W. Ludwig, Paramagnetic resonance study of a deep donor in silicon, *Phys. Rev.* 137 (1965) 1520.
- [28] E. Janzén, R. Stedman, G. Grossmann, H.G. Grimmeiss, High-resolution studies of sulfur- and selenium-related donor centers in silicon, *Phys. Rev. B* 29 (1984) 1907.
- [29] M.J. Smith, Y.T. Lin, M.J. Sher, M.T. Winkler, E. Mazur, S. Gradečak, Pressure-induced phase transformations during femtosecond-laser doping of silicon, *J. Appl. Phys.* 110 (2011) 053524.
- [30] B.D. Malone, J.D. Sau, M.L. Cohen, Ab initio study of the optical properties of Si-XII, *Phys. Rev. B* 78 (2008) 161202.
- [31] G. Weill, J.L. Mansot, G. Sagon, C. Carlone, J.M. Besson, Characterisation of Si III and Si IV, metastable forms of silicon at ambient pressure, *Semicond. Sci. Technol.* 4 (1989) 280.
- [32] B. Franta, D. Pastor, H.H. Gandhi, P.H. Rekemeyer, S. Gradečak, M.J. Aziz, E. Mazur, Simultaneous high crystallinity and sub-bandgap optical absorbance in hyperdoped black silicon using nanosecond laser annealing, *J. Appl. Phys.* 118 (2015) 225303.